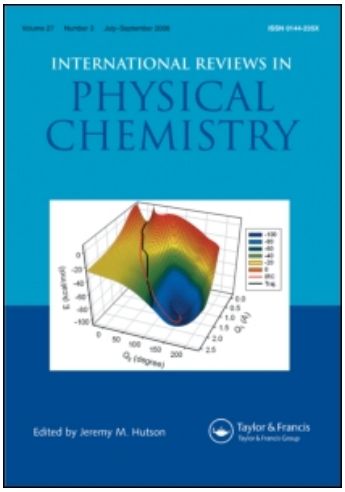

International Reviews in Physical Chemistry
Publication details, including instructions for authors and subscription information:
http://www.informaworld.com/smpp/title~content=t713724383

Hybrid approach for the dynamical simulation of proton and hydride transfer in solution and proteins

Sharon Hammes-Schiffer; Salomon R. Billeter

Online publication date: 26 November 2010

To cite this Article Hammes-Schiffer, Sharon and Billeter, Salomon R.(2001) 'Hybrid approach for the dynamical simulation of proton and hydride transfer in solution and proteins', International Reviews in Physical Chemistry, 20: 4, 591 — 616
To link to this Article: DOI: 10.1080/01442350110067402
URL: http://dx.doi.org/10.1080/01442350110067402

INT. REVIEWS IN PHYSICAL CHEMISTRY, 2001, VOL. 20, NO. 4, 591–616

Hybrid approach for the dynamical simulation of proton and hydride transfer in solution and proteins

SHARON HAMMES-SCHIFFER† and SALOMON R. BILLETER
Department of Chemistry, 152 Davey Laboratory, Pennsylvania State University, University Park, PA 16802, USA

A hybrid approach for simulating proton and hydride transfer reactions in solution and proteins is described. The electronic quantum effects are incorporated with an empirical valence bond potential. The nuclear quantum effects are included with a mixed quantum–classical molecular dynamics method in which the transferring hydrogen nuclei are represented by multidimensional vibrational wavefunctions. The free energy profiles are obtained as functions of a collective reaction coordinate, and a mapping or umbrella potential is utilized to drive the reaction over the barrier for infrequent events. The vibrationally adiabatic nuclear quantum effects are incorporated into the free energy profiles. The dynamics are described with the molecular dynamics with quantum transitions (MDQT) surface hopping method, which incorporates vibrationally non-adiabatic effects. The MDQT method is combined with a reactive flux approach to calculate the transmission coefficient and to investigate the real-time dynamics of reactive trajectories. Nuclear quantum effects such as zero point energy, hydrogen tunnelling and non-adiabatic transitions, as well as the dynamics of the solvent and protein environment, are included during the generation of the free energy profiles and dynamical trajectories. This methodology provides detailed mechanistic information at the molecular level and allows the calculation of rates and kinetic isotope effects. The feasibility of this approach is illustrated through an application to hydride transfer in the enzyme liver alcohol dehydrogenase. This approach may be extended for use with mixed quantum mechanical–molecular mechanical potentials and alternative mixed quantum–classical molecular dynamics methods. It has also been generalized for multiple proton and proton-coupled electron transfer reactions.

Contents

† E-mail: shs@chem.psu.edu

International Reviews in Physical Chemistry ISSN 0144–235X print/ISSN 1366–591X online © 2001 Taylor & Francis Ltd
http://www.tandf.co.uk/journals
DOI: 10.1080/01442350110067402

1. Introduction

Proton and hydride transfer reactions play a vital role in a wide range of chemical and biological processes. The simulation of these reactions is challenging due to the importance of both electronic and nuclear quantum effects, as well as the dynamics of the solvent and protein environment. The incorporation of electronic quantum effects is required for the description of the breaking and forming of chemical bonds. Nuclear quantum effects such as zero point energy, hydrogen tunnelling, and non-adiabatic transitions have also been found to be significant for proton and hydride transfer reactions [1, 2]. In addition, recent experiments have suggested a significant impact of enzyme dynamics on hydride transfer reactions [3–5].

Numerous approaches have been utilized to study proton and hydride transfer reactions in solution and enzymes. One approach is the use of classical molecular dynamics simulations with molecular mechanical (MM) force fields [6, 7]. This approach may elucidate dynamical aspects of reactant or product states, but it is unable to probe the dynamical reaction path since MM force fields do not allow bonds to break and form. Moreover, the nuclear quantum effects are not included in standard classical molecular dynamics simulations. A variety of methods have been developed to include the electronic and nuclear quantum effects in simulations of proton and hydride transfer reactions.

Electronic quantum effects may be incorporated into these types of simulation by the use of mixed quantum mechanical–molecular-mechanical (QM–MM) potentials [8–12] or empirical valence bond (EVB) potentials [13, 14]. In QM–MM methods, the system is divided into reactive and non-reactive portions. The reactive portion of the system is treated quantum mechanically with semiempirical or *ab initio* methods, while the non-reactive portion of the system is represented by a standard MM potential. The various QM–MM methods differ mainly in the treatment of the boundary between the QM and MM portions. The alternative EVB potential describes the reaction in terms of a small number of resonance structures (i.e. valence bond (VB) states). The matrix elements between these VB states are represented as MM terms fitted to electronic structure calculations or experimental data. In contrast with the QM–MM methods, the EVB potential [13] does not require a partitioning between the QM and MM portions of the system. Moreover, the EVB method is conceptually straightforward and often is nearly as computa-

tionally efficient as a standard potential. Both EVB and QM–MM potentials have been used in conjunction with classical molecular dynamics simulations to study proton transfer in solution and enzymes [15, 16]. Recently, a promising mixed molecular orbital–valence bond (MO–VB) method has been developed and applied to proton transfer in solution [17]. Although the EVB, QM–MM, and MO–VB potentials allow bonds to break and form, these simulations did not include nuclear quantum effects such as zero point energy and hydrogen tunnelling.

One powerful approach for incorporating nuclear quantum effects is the use of centroid path integral methods. Many groups have used centroid path integral methods to study equilibrium properties of proton transfer reactions in solution [18–26] and enzymes [18–21]. This equilibrium centroid path integral approach, however, does not describe non-equilibrium dynamical properties. Cao and Voth [27–30] have developed the centroid molecular dynamics method to allow the study of dynamical properties and Schmitt and Voth [31] have applied this method to proton transfer in bulk water. Furthermore, recently several semiclassical methods have been developed and applied to gas-phase [32, 33] and model solvated proton transfer reactions [34, 35].

An alternative to the path integral approach is the mixed quantum–classical molecular dynamics approach, in which the transferring hydrogen nucleus is represented by a QM wavefunction, while the other nuclei are treated classically. The advantage of this approach is that it directly provides real-time dynamical information. A variety of different mixed quantum–classical methods have been developed and applied to proton and hydride transfer reactions [18–23, 36–55]. Most of these applications involved only the one-dimensional motion of a single hydrogen nucleus. Recently, these methods have been applied to reactions involving three-dimensional motion of a single hydrogen nucleus [56] and to multiple hydrogen nuclei [57, 58]. These extensions required the development of methodology for the efficient and accurate calculation of multidimensional vibrational wavefunctions [59].

The various mixed quantum–classical methods differ in the treatment of the interactions between the quantum and classical subsystems. In the adiabatic method, the classical subsystem moves on a single adiabatic surface (typically the hydrogen vibrational ground state). Several groups have used the adiabatic method to simulate proton transfer in solution [23, 39–42]. This method is valid only in the adiabatic limit (i.e. when the proton transfer barrier is low).

Numerous methods have been developed to include vibrationally non-adiabatic effects in simulations. In the mean field methods, the classical subsystem follows an average path derived from a mixture of adiabatic states. Mean field methods have been used for the simulation of proton transfer in enzymes [47–49]. The mean field methods are useful in the adiabatic and non-adiabatic limits or when the adiabatic states exert similar forces on the classical subsystem. For typical proton and hydride transfer reactions, however, the adiabatic states have qualitatively different charge distributions and thus exert different forces on the classical subsystem. Surface hopping methods were designed to describe processes that end up in a mixture of adiabatic states exerting different forces on the classical subsystem [50, 60–78]. In surface hopping methods, the classical subsystem moves according to a force derived from a single adiabatic state with the possibility of non-adiabatic transitions among the adiabatic states. Surface hopping methods have been used to simulate proton transfer reactions in solution [50, 52] and enzymes [56]. In [79] it was shown that

surface hopping describes branching processes more accurately than mean field methods do for one-dimensional model proton transfer systems. Since mean field methods are advantageous for processes involving long times in strong non-adiabatic coupling regions or a large number of repeated entrances into such regions, recently an approach that combines surface hopping and mean field methods has been developed [80, 81]. To date, this combined method has not yet been applied to proton transfer reactions.

A variety of other approaches have also been applied to proton and hydride transfer in solution and enzymes. For example, the combination of the Car–Parrinello *ab initio* molecular dynamics method with equilibrium centroid path integral calculations has been applied to proton transfer in water [25, 26]. These simulations provide useful information about equilibrium properties but do not allow the study of non-equilibrium dynamical properties. Another approach is the calculation of semiclassical tunnelling corrections to a minimum energy reaction path obtained with a QM–MM potential for proton and hydride transfer in enzymes [82, 83]. Although these calculations include both electronic and nuclear quantum effects, they do not include the dynamics of the majority of the enzyme during the generation of the reaction path or the subsequent calculation of the tunnelling corrections.

This review describes a hybrid approach for the real-time dynamical simulation of proton and hydride transfer reactions in enzymes. The electronic quantum effects are incorporated with an EVB potential, and the nuclear quantum effects of the transferring hydrogen are incorporated with the mixed quantum–classical molecular dynamics with quantum transitions (MDQT) surface hopping method. This approach allows the calculation of rates and kinetic isotope effects, as well as the analysis of real-time dynamical trajectories. The procedure for obtaining the rates involves the calculation of both a transition state theory rate constant determined from a free energy profile and a transmission coefficient determined from an ensemble of real-time MDQT trajectories.

The transition state theory rate constant is calculated from the expression

$$k_{\mathrm{TST}} = \frac{k_{\mathrm{B}}T}{h}\exp\left(\frac{-\Delta G^{\dagger}}{k_{\mathrm{B}}T}\right), \tag{1}$$

where $\Delta G^{\dagger}$ is the free energy barrier for the reaction and k_{B} is Boltzmann's constant. For the hybrid approach described in this review, the free energy barrier is determined from free energy profiles that depend on a collective reaction coordinate analogous to the solvent coordinate in Marcus theory for electron transfer (ET) [14, 84–86]. A mapping or umbrella potential is used to drive the reaction over the barrier for infrequent events. The free energy profiles are calculated from molecular dynamics simulations with a combination of perturbation formulae and thermodynamic integration. The vibrationally adiabatic nuclear quantum effects are included during the generation of these free energy profiles by representing the transferring hydrogen nuclei as multidimensional vibrational wavefunctions.

The transition state theory rate constant k_{TST} defined in equation (1) is based on the assumption that the rate is determined by the forward flux through the dividing surface (i.e. each trajectory passes through the dividing surface only one time). In dynamical systems, the environment may cause trajectories to recross the

dividing surface. The 'exact' rate constant k_{dyn} including dynamical effects may be expressed as

$$k_{dyn} = \kappa k_{TST}, \tag{2}$$

where κ is the transmission coefficient that accounts for recrossings of the dividing surface. In standard classical molecular dynamics simulations, κ may be calculated using reactive flux methods for infrequent events [87–90]. The reactive flux scheme involves initiating a canonical ensemble of trajectories at the dividing surface and propagating them backwards and forwards in time to determine the extent of barrier recrossing. For the hybrid approach described in this review, the vibrationally non-adiabatic nuclear quantum effects are included in the calculation of κ by combining the MDQT surface hopping method with this reactive flux scheme. This approach allows the analysis of real-time reactive trajectories in the presence of a fully dynamical solvent and protein environment.

In addition to presenting this hybrid approach, this review summarizes the results from an initial application to hydride transfer in liver alcohol dehydrogenase (LADH). LADH catalyses the reversible oxidation of alcohols to aldehydes or ketones by the coenzyme nicotinamide dinucleotide (NAD^+). This enzyme was chosen as the prototype for testing this methodology because of its biochemical importance, the availability of a high-resolution crystal structure [91, 92] and experimental kinetic isotope effect experiments indicating significant hydrogen tunnelling [1, 2, 93]. The rates and kinetic isotope effects were calculated for this system, and the physical basis for the results were analysed in terms of changes in the free energy barrier and transmission coefficient. In addition, correlation functions between specific geometrical properties of the system and the degree of dynamical barrier recrossing were calculated to elucidate the dynamical role of the enzyme. These simulations provide insight into the relation between enzyme dynamics and enzyme function.

Furthermore, this review presents the extension of this hybrid approach to multiple charge transfer reactions, namely double proton transfer and proton-coupled ET (PCET). (In this review, PCET refers to the transfer of one electron and one proton.) As shown in [94], typically a process involving N charge transfer reactions may be described in terms of 2^N VB states and N collective reaction coordinates. Within this framework, double proton transfer and PCET are described in terms of four VB states and two collective reaction coordinates. The calculation of the two-dimensional free energy surfaces for these types of reaction is analogous to the calculation of the one-dimensional free energy profiles for single proton and hydride transfer. For the case of double proton transfer, the hydrogen vibrational wavefunctions depend on two nuclear coordinates rather than on only one. For the case of PCET, the ET reaction is typically electronically non-adiabatic, leading to the generation of mixed electronic–vibrational free energy surfaces for each ET state. The rates and kinetic isotope effects may be calculated for both types of reaction. In addition, the detailed mechanisms, such as whether the charge transfer reactions are concerted or sequential, may be determined from an analysis of the two-dimensional free energy surfaces and the real-time dynamical trajectories.

An outline of this review is as follows. Section 2 describes the hybrid approach for the dynamical simulation of proton and hydride transfer reactions. In section 2.1 the incorporation of the electronic and nuclear quantum effects is described. Section 2.2 presents the methods for calculating the free energy surfaces as functions of a

collective reaction coordinate, including the vibrationally adiabatic nuclear quantum effects. Section 2.3 presents the approach for calculating dynamical effects combining a reactive flux method for infrequent events with the mixed quantum–classical MDQT surface hopping approach. Section 3 describes the results of the initial application of this methodology to LADH and the extensions to double proton transfer and PCET reactions. Section 4 summarizes this approach and discusses future directions.

2. Methodology

2.1. *Two levels of quantum mechanics*

The simulation of proton and hydride transfer reactions entails the incorporation of both electronic and nuclear quantum effects. The electronic quantum effects are required to describe the breaking and forming of chemical bonds. The nuclear quantum effects of the transferring hydrogen nuclei are required to include properties such as zero point energy and hydrogen tunnelling.

2.1.1. *Electronic quantum effects*

The total Hamiltonian for a system with electronic coordinates $\mathbf{R}_{\mathrm{el}}$ and nuclear coordinates $\mathbf{R}_{\mathrm{nuc}}$ is

$$H_{\mathrm{tot}} = T_{\mathrm{nuc}} + T_{\mathrm{el}} + V(\mathbf{R}_{\mathrm{el}}, \mathbf{R}_{\mathrm{nuc}}), \tag{3}$$

where T_{nuc} and T_{el} represent the kinetic energies of the nuclei and electrons respectively and V is the total potential energy of the system. (For notational simplicity, the explicit dependence of the Hamiltonian on the coordinates and momenta is omitted.) For an electronically adiabatic reaction, a Born–Oppenheimer separation of the electrons and nuclei may be applied. In this case, the electronic Hamiltonian is defined as

$$H_{\mathrm{el}} = T_{\mathrm{el}} + V(\mathbf{R}_{\mathrm{el}}, \mathbf{R}_{\mathrm{nuc}}), \tag{4}$$

and the nuclei are assumed to move on the potential energy surface $V_{\mathrm{el0}}(\mathbf{R}_{\mathrm{nuc}})$ defined as the lowest eigenvalue of the solution of the electronic time-independent Schrödinger equation:

$$H_{\mathrm{el}}\chi_0(\mathbf{R}_{\mathrm{el}}; \mathbf{R}_{\mathrm{nuc}}) = V_{\mathrm{el0}}(\mathbf{R}_{\mathrm{nuc}})\chi_0(\mathbf{R}_{\mathrm{el}}; \mathbf{R}_{\mathrm{nuc}}). \tag{5}$$

This potential energy surface corresponds to the electronic ground state. As described in the introduction, a variety of methods have been developed to incorporate the electronic quantum effects in the potential energy surface $V_{\mathrm{el0}}(\mathbf{R}_{\mathrm{nuc}})$. The hybrid approach described in this review centres on the EVB potential, although the extension for use with a QM–MM potential will also be discussed.

In the EVB method, equation (5) is solved by expanding the wavefunction $\chi_0(\mathbf{R}_{\mathrm{el}}; \mathbf{R}_{\mathrm{nuc}})$ in a basis of N_{VB} VB states $\phi_i(\mathbf{R}_{\mathrm{el}})$. (For the simplest description of a proton or hydride transfer reaction, only two VB states are required.) The electronic Hamiltonian matrix $\tilde{\mathbf{H}}_{\mathrm{el}}$ in this basis set has matrix elements $V_{ij}(\mathbf{R}_{\mathrm{nuc}}) = \langle \phi_i | H_{\mathrm{el}} | \phi_j \rangle_{\mathbf{R}_{\mathrm{el}}}$ with $\langle \ldots \rangle_{\mathbf{R}_{\mathrm{el}}}$ indicating integration over the electronic coordinates $\mathbf{R}_{\mathrm{el}}$. In this basis set, equation (5) becomes

$$\tilde{\mathbf{H}}_{\mathrm{el}}\mathbf{c}_0(\mathbf{R}_{\mathrm{nuc}}) = V_{\mathrm{el0}}(\mathbf{R}_{\mathrm{nuc}})\mathbf{c}_0(\mathbf{R}_{\mathrm{nuc}}), \tag{6}$$

where $\mathbf{c}_0(\mathbf{R}_{\text{nuc}})$ is an N_{VB}-dimensional vector containing the coefficients of the two VB states for the electronic ground state wavefunction:

$$\chi_0(\mathbf{R}_{\text{el}};\mathbf{R}_{\text{nuc}}) = \sum_{i=0}^{N_{\text{VB}}-1} c_{0i}(\mathbf{R}_{\text{nuc}})\phi_i(\mathbf{R}_{\text{el}}). \tag{7}$$

The electronic ground state potential energy surface $V_{\text{el}0}(\mathbf{R}_{\text{nuc}})$ is obtained by diagonalization of $\tilde{\mathbf{H}}_{\text{el}}$. Typically the matrix elements $V_{ij}(\mathbf{R}_{\text{nuc}})$ are represented as analytical functional forms containing parameters fit to electronic structure calculations or experimental data.

2.1.2. *Nuclear quantum effects*

In addition to these electronic quantum effects, the nuclear quantum effects of the transferring hydrogen atom(s) must be incorporated into simulations of hydrogen transfer reactions. For condensed-phase systems, this requires a mixed quantum–classical description of the nuclei, in which the nuclear coordinates are divided into the quantum coordinates $\mathbf{r}$ and the classical coordinates $\mathbf{R}$: $\mathbf{R}_{\text{nuc}} = (\mathbf{r},\mathbf{R})$. In the simplest case, only the transferring hydrogen nuclei are treated quantum mechanically. The total nuclear Hamiltonian can be expressed as

$$H_{\text{nuc}} = T_{\text{nuc}}^{\text{quant}} + T_{\text{nuc}}^{\text{class}} + V_{\text{el}0}(\mathbf{r},\mathbf{R}), \tag{8}$$

where $T_{\text{nuc}}^{\text{quant}}$ and $T_{\text{nuc}}^{\text{class}}$ are the kinetic energies for the quantum and classical nuclei respectively. The adiabatic vibrational wavefunctions for the quantum nuclei can be calculated for fixed classical coordinates $\mathbf{R}$ by solving the time-independent Schrödinger equation

$$H_{\text{nuc}}^{\text{quant}}\Phi_n(\mathbf{r};\mathbf{R}) = \epsilon_n(\mathbf{R})\Phi_n(\mathbf{r};\mathbf{R}), \tag{9}$$

where

$$H_{\text{nuc}}^{\text{quant}} = T_{\text{nuc}}^{\text{quant}} + V_{\text{el}0}(\mathbf{r},\mathbf{R}). \tag{10}$$

When non-adiabatic effects from the excited vibrational states are required, equation (9) must be solved for a range of states n.

A variety of methods have been developed to calculate the adiabatic vibrational wavefunctions (i.e. to solve equation (9)). The use of analytical basis functions such as Hermite polynomials is problematic owing to the computational expense of the required numerical integration of the potential energy matrix elements and the bias introduced by the choice of the centres and parameters associated with the basis functions. The use of a grid basis set is advantageous since the costly calculation of multidimensional integrals is avoided and the entire range of hydrogen coordinates is treated without bias. The computational expense for the diagonalization of large matrices required for a grid basis set is significantly decreased through the use of iterative methods such as the Lanczos [95], the Davidson [96] and other related schemes [97–102]. The recently developed Fourier grid Hamiltonian multiconfigurational self-consistent field (FGH-MCSCF) method has been shown to be particularly efficient for the calculation of multidimensional hydrogen vibrational wavefunctions [59].

In the FGH-MCSCF method, a vibrational wavefunction is expressed as a linear combination of N_{config} single configurations, which are products of one-dimensional wavefunctions:

$$\Phi_n(\mathbf{r};\mathbf{R}) = \sum_{I}^{N_{\text{config}}} \left(C_I^n(\mathbf{R}) \prod_{p}^{N_{\text{dim}}} \psi_{i_p}^{(p)}(r_p;\mathbf{R}) \right), \tag{11}$$

where N_{dim} is the dimension of the quantum coordinate, $\mathbf{r} = (r_1, r_2, \ldots, r_{N_{\text{dim}}})$, and the index $I = (i_1, i_2, \ldots, i_{N_{\text{dim}}})$. For fixed classical coordinates $\mathbf{R}$, the variational method is utilized to optimize the wavefunction $\Phi_n(\mathbf{r};\mathbf{R})$ with respect to the coefficients of the configurations $C_I^n(\mathbf{R})$ and the one-dimensional wavefunctions $\psi_{i_p}^{(p)}(r_p;\mathbf{R})$. A full configuration interaction calculation is carried out in a truncated one-dimensional wavefunction space (analogous to complete active space self-consistent-field in electronic structure theory). If multiple states are required, a state-averaged approach is used to obtain a set of orthogonal multidimensional vibrational wavefunctions. The one-dimensional wavefunctions are represented directly on a grid with N_{grid} points in each dimension, and the kinetic energy matrix elements are calculated with Fourier methods. This FGH-MCSCF approach avoids the expensive diagonalization of large matrices and accurately describes ground and excited state hydrogen vibrational wavefunctions.

Although methods such as the FGH-MCSCF method decrease the computational expense of calculating the vibrational wavefunctions, these types of grid method require the calculation of the potential energy and forces at each grid point. This calculation of the grid potential for each molecular dynamics time step is often the bottleneck of mixed quantum–classical molecular dynamics simulations. The calculation of this grid potential is more efficient for an EVB potential than for a standard QM–MM potential since the calculation of an EVB grid potential requires only a single calculation of the complete potential energy for each time step (as well as the much faster calculation of only the terms involving the quantum hydrogen nuclei for each grid point). To decrease further the computational expense of the calculation of the grid potential, recently a partial multidimensional grid generation method was developed [103]. This method substantially decreases the number of potential energy calculations (typically by more than an order of magnitude) by avoiding these calculations for grid points with high potential energy.

2.2. *Free energy profiles*

2.2.1. *Fundamental aspects of free energy profiles*

As discussed in the introduction, in order to calculate the transition state theory rate constant defined in equation (1), the free energy profile must be calculated. For simplicity, first we describe the calculation of the free energy profiles in terms of an EVB potential. At the end of this section, this formulation will be generalized for use with QM–MM potentials.

For reactions involving a free energy barrier that is significantly larger than the thermal energy, the system must be driven over the barrier with a mapping or umbrella potential. Within the two-state EVB formulation, a mapping potential $V_{\text{map}}(\mathbf{r},\mathbf{R};\lambda)$ may be defined as

$$V_{\text{map}}(\mathbf{r},\mathbf{R};\lambda) = (1-\lambda)V_{11}(\mathbf{r},\mathbf{R}) + \lambda V_{22}(\mathbf{r},\mathbf{R}), \tag{12}$$

where V_{11} and V_{22} are the diagonal elements of the EVB Hamiltonian. As the parameter λ is varied from zero to unity, the reaction progresses from the reactant VB state 1 to the product VB state 2. The alternative use of an umbrella potential will be discussed below.

A variety of reaction coordinates have been used to describe proton and hydride transfer reactions. When the transferring hydrogen is treated classically, a physically meaningful reaction coordinate is the collective reaction coordinate

$$\Lambda^{(c)}(\mathbf{r},\mathbf{R}) = V_{22}(\mathbf{r},\mathbf{R}) - V_{11}(\mathbf{r},\mathbf{R}). \tag{13}$$

This collective reaction coordinate is similar to the solvent coordinate used in standard Marcus theory for ET reactions [14, 84–86]. This classical reaction coordinate depends on both **r** and **R**. When the transferring hydrogen is treated quantum-mechanically in mixed quantum–classical molecular dynamics simulations, however, the reaction coordinate should not be a function of the quantum coordinate **r** since the classical molecular dynamics samples the configurational space of only the classical coordinates **R**. Moreover, the reaction coordinate $\Lambda^{(c)}(\mathbf{r},\mathbf{R})$ defined in equation (13) does not distinguish between symmetric and asymmetric hydrogen potential energy surfaces (or hydrogen vibrational wavefunctions), as required in the framework of standard Marcus theory [84]. A quantum reaction coordinate analogous to the classical collective reaction coordinate given above is

$$\Lambda^{(q)}(\mathbf{R}) = \langle \Phi_0(\mathbf{r};\mathbf{R}) | V_{22}(\mathbf{r},\mathbf{R}) - V_{11}(\mathbf{r},\mathbf{R}) | \Phi_0(\mathbf{r};\mathbf{R}) \rangle_{\mathbf{r}}, \tag{14}$$

where $\langle \ldots \rangle_{\mathbf{r}}$ indicates integration over the quantum coordinate **r** and $\Phi_0(\mathbf{r};\mathbf{R})$ is the ground state vibrational wavefunction. Note that, in practice, the classical and quantum reaction coordinates are divided into discrete intervals (i.e. bins) represented by values Λ_n.

2.2.2. *Classical free energy profile*

The calculation of the classical free energy profile for the electronic ground state potential $V_{el0}(\mathbf{r},\mathbf{R})$ consists of three steps. In the first step, the free energy $F_{map}(\Lambda_n;\lambda_m)$ for the mapping potential along the reaction coordinate $\Lambda^{(c)}(\mathbf{r},\mathbf{R})$ defined in equation (13) is calculated for each λ_m from the formula

$$\exp[-\beta F_{map}(\Lambda_n;\lambda_m)] = C_{map}(\lambda_m)\langle \delta(\Lambda^{(c)}(\mathbf{r},\mathbf{R}) - \Lambda_n)\rangle_{\lambda_m}, \tag{15}$$

where

$$\langle f(\mathbf{r},\mathbf{R})\rangle_{\lambda_m} = \frac{\int d\mathbf{r} \int d\mathbf{R} f(\mathbf{r},\mathbf{R}) \exp[-\beta V_{map}(\mathbf{r},\mathbf{R};\lambda_m)]}{\int d\mathbf{r} \int d\mathbf{R} \exp[-\beta V_{map}(\mathbf{r},\mathbf{R};\lambda_m)]} \tag{16}$$

and $\delta(\Lambda^{(c)}(\mathbf{r},\mathbf{R}) - \Lambda_n)$ is a unitless quantity equal to unity if $\Lambda^{(c)}(\mathbf{r},\mathbf{R})$ is within the bin represented by Λ_n and zero otherwise. In practice, $\langle \delta(\Lambda^{(c)}(\mathbf{r},\mathbf{R}) - \Lambda_n)\rangle_{\lambda_m}$ is calculated using a standard binning procedure during molecular dynamics simulations governed by $V_{map}(\mathbf{r},\mathbf{R};\lambda_m)$.

In the second step, the relative free energies for the mapping potential corresponding to the same value of Λ_n but different values of λ_m are determined by calulating the factors $C_{map}(\lambda_m)$ from the relation

$$C_{map}(\lambda_m) = \frac{\exp[-\beta F_{maptot}(\lambda_m)]}{\sum_n \langle \delta(\Lambda^{(c)}(\mathbf{r},\mathbf{R}) - \Lambda_n)\rangle_{\lambda_m}}. \tag{17}$$

This relation is derived from the identity

$$\exp[-\beta F_{maptot}(\lambda_m)] = \sum_n \exp[-\beta F_{map}(\Lambda_n;\lambda_m)], \tag{18}$$

where $\sum_n$ is a summation over all bins representing relevant values of Λ_n and the free energy $F_{\mathrm{maptot}}(\lambda_m)$ is calculated using thermodynamic integration:

$$F_{\mathrm{maptot}}(\lambda_m) - F_{\mathrm{maptot}}(\lambda_1) = \sum_{m'=1}^{m} \Delta\lambda_{m'} \left\langle \left. \frac{\partial V_{\mathrm{map}}(\mathbf{r}, \mathbf{R}; \lambda)}{\partial \lambda} \right|_{\lambda_{m'}} \right\rangle_{\lambda_{m'}}. \tag{19}$$

Note that this procedure avoids the arbitrary translation of the individual segments of the free energy profile corresponding to different values of λ_m. Moreover, the degree of overlap of the neighbouring segments provides an indication of the convergence of the calculation.

In the third step of this procedure, the classical free energy $F_{\mathrm{el0}}(\Lambda_n; \lambda_m)$ for the electronic ground state potential $V_{\mathrm{el0}}(\mathbf{r}, \mathbf{R})$ is calculated using a perturbation formula [13, 104]

$$\exp[-\beta F_{\mathrm{el0}}(\Lambda_n; \lambda_m)] = \exp[-\beta F_{\mathrm{map}}(\Lambda_n; \lambda_m)] \times \langle \exp\{-\beta[V_{\mathrm{el0}}(\mathbf{r}, \mathbf{R}) - V_{\mathrm{map}}(\mathbf{r}, \mathbf{R}; \lambda_m)]\}\rangle_{\lambda_m, \Lambda_n, c} \tag{20}$$

where

$$\langle f(\mathbf{r}, \mathbf{R})\rangle_{\lambda_m, \Lambda_n, c} = \frac{\int \mathrm{d}\mathbf{r} \int \mathrm{d}\mathbf{R}\, \delta(\Lambda^{(\mathrm{c})}(\mathbf{r}, \mathbf{R}) - \Lambda_n) f(\mathbf{r}, \mathbf{R}) \exp[-\beta V_{\mathrm{map}}(\mathbf{r}, \mathbf{R}; \lambda_m)]}{\int \mathrm{d}\mathbf{r} \int \mathrm{d}\mathbf{R}\, \delta(\Lambda^{(\mathrm{c})}(\mathbf{r}, \mathbf{R}) - \Lambda_n) \exp[-\beta V_{\mathrm{map}}(\mathbf{r}, \mathbf{R}; \lambda_m)]}. \tag{21}$$

The quantity in angular brackets is calculated within the bins used in equation (15) during molecular dynamics simulations governed by the mapping potential $V_{\mathrm{map}}(\mathbf{r}, \mathbf{R}; \lambda_m)$. (Note that, for convenience, this binning procedure may be performed after the simulations.)

2.2.3. *Quantum free energy profile*

For the generation of the quantum free energy profile, the vibrationally adiabatic nuclear quantum effects are included. The quantum free energy $F_{\mathrm{el0,nuc0}}(\Lambda_n; \lambda_m)$ associated with the energy of the ground-state hydrogen vibrational wavefunction (defined as $\epsilon_0(\mathbf{R})$ in equation (9)) may be calculated from the perturbation formula

$$\exp[-\beta F_{\mathrm{el0,nuc0}}(\Lambda_n; \lambda_m)] = \exp[-\beta F_{\mathrm{map}}(\Lambda_n; \lambda_m)] \times \langle \exp\{-\beta[\epsilon_0(\mathbf{R}) - V_{\mathrm{intmap}}(\mathbf{R}; \lambda_m)]\}\rangle_{\lambda_m, \Lambda_n, q}. \tag{22}$$

Here $\langle \ldots \rangle_{\lambda_m, \Lambda_n, q}$ is defined as in equation (21) with $\Lambda^{(\mathrm{c})}(\mathbf{r}, \mathbf{R})$ replaced by $\Lambda^{(\mathrm{q})}(\mathbf{R})$, and

$$\exp[-\beta V_{\mathrm{intmap}}(\mathbf{R}; \lambda_m)] = C_{\mathbf{r}} \int \mathrm{d}\mathbf{r} \exp[-\beta V_{\mathrm{map}}(\mathbf{r}, \mathbf{R}; \lambda_m)], \tag{23}$$

where $C_{\mathbf{r}}$ is a constant of dimension inverse volume in the coordinate space $\mathbf{r}$. The derivation of this perturbation formula is given in [56]. (Note that the constant $C_{\mathbf{r}}$ does not affect the relative quantum free energies for different values of Λ_n and λ_m. For comparison between the classical and quantum free energies, however, $C_{\mathbf{r}}$ is set to $h^{-3} \int \mathrm{d}\mathbf{p} \exp(-\beta \mathbf{p}^2/2m)$, where h is Planck's constant and m is the mass of a hydrogen atom.)

2.2.4. *Extensions of free energy formulation*

The formulation described above may be generalized for use with a QM–MM potential. In this case, the classical reaction coordinate could be the position of the transferring hydrogen relative to the donor and acceptor, and the quantum reaction

coordinate could be $\langle \Phi_0(\mathbf{r};\mathbf{R})|\mathbf{r}|\Phi_0(\mathbf{r};\mathbf{R})\rangle_p$. Another possibility would be to define a quantum reaction coordinate analogous to equation (14) as the energy difference between the hydrogen bonded to its donor and to its acceptor (calculated with all other nuclei fixed). These alternative reaction coordinates would require testing to ensure that they effectively distinguish between symmetric and asymmetric hydrogen potential energy surfaces (or hydrogen vibrational wavefunctions).

When a QM–MM potential is used to simulate infrequent events, the reaction could be driven over the barrier with an umbrella potential rather than a mapping potential. For example, an umbrella potential could be defined as

$$V_{\text{umb}}(\mathbf{r},\mathbf{R};\Gamma_m) = V_{\text{el0}}(\mathbf{r},\mathbf{R}) + K[\Gamma(\mathbf{r},\mathbf{R}) - \Gamma_m]^2, \tag{24}$$

where K is a specified constant and $\Gamma(\mathbf{r},\mathbf{R})$ is a general function that may be defined as a geometrical coordinate or a collective reaction coordinate. The free energy surfaces could be calculated with the formulation described above by replacing V_{map} with V_{umb}.

2.3. *Dynamical effects*

2.3.1. *Fundamental aspects of dynamical effects*

As discussed in the introduction, the 'exact' rate constant k_{dyn} including dynamical effects is the product of the transition state theory rate constant and the transmission coefficient κ, which accounts for recrossings of the dividing surface. In standard classical molecular dynamics simulations, κ may be calculated using reactive flux methods for infrequent events [87–90]. In this scheme, κ is calculated as the flux-weighted average of a quantity ξ for a canonical ensemble of classical molecular dynamics trajectories started at the dividing surface and integrated backwards and forwards in time. The quantity ξ corrects for multiple crossings of the dividing surface (i.e. so that all trajectories that originate as reactants and end as products are counted only once, no matter how many times they cross the dividing surface, and all trajectories that go from reactants to reactants, from products to products, or from products to reactants are not counted at all). In particular, $\xi = 1/\alpha$ for trajectories that have α forward crossings and $\alpha - 1$ backward crossings of the dividing surface, and ξ is zero otherwise.

The nuclear quantum effects may be incorporated into the calculation of κ by combining a mixed quantum–classical molecular dynamics method with this reactive flux method for infrequent events. As discussed in the introduction, a variety of mixed quantum–classical molecular dynamics methods have been developed and applied to proton and hydride transfer reactions in solution and enzymes. This review focuses on the combination of the MDQT surface hopping method with the reactive flux scheme for infrequent events. At the end of this section, the generalization to other mixed quantum–classical molecular dynamics methods will be discussed.

2.3.2. *Molecular dynamics with quantum transitions*

The fundamental principle of the MDQT method [50, 52, 60] is that an ensemble of trajectories is propagated, and each trajectory moves classically on a single adiabatic surface except for instantaneous transitions among the adiabatic states. The adiabatic states $\Phi_n(\mathbf{r};\mathbf{R})$ are calculated at each classical molecular dynamics time step by solving equation (9) with a method such as the Lanczos [95], Davidson [96] or

FGH-MCSCF [59] scheme. The time-dependent wavefunction describing the quantum nuclei is expanded in a basis of the N_{ad} lowest-energy adiabatic states:

$$\Psi(\mathbf{r},\mathbf{R},t) = \sum_{n=0}^{N_{\mathrm{ad}}-1} C_n(t)\Phi_n(\mathbf{r};\mathbf{R}). \tag{25}$$

The surface hopping algorithm is designed to apportion trajectories correctly among the adiabatic states according to the quantum probabilities $|C_n(t)|^2$.

The classical nuclei evolve according to Newton's classical equations of motion with the effective potential

$$V_{\mathrm{eff}}(\mathbf{R}) = \epsilon_k(\mathbf{R}), \tag{26}$$

where k denotes the occupied adiabatic state and $\epsilon_k(\mathbf{R})$ is defined in equation (9). The Hellmann–Feynman theorem can be utilized to obtain the corresponding effective force

$$\mathbf{F}_{\mathrm{eff}} = -\nabla_{\mathbf{R}}\epsilon_k(\mathbf{R}) = -\langle\Phi_k|\nabla_{\mathbf{R}}V_{\mathrm{el0}}(\mathbf{r},\mathbf{R})|\Phi_k\rangle_{\mathbf{r}}. \tag{27}$$

Within the EVB description,

$$\nabla_{\mathbf{R}}V_{\mathrm{el0}}(\mathbf{r},\mathbf{R}) = \sum_{i=0}^{N_{\mathrm{VB}}-1}\sum_{j=0}^{N_{\mathrm{VB}}-1} c_{0i}(\mathbf{r},\mathbf{R})c_{0j}(\mathbf{r},\mathbf{R})\nabla_{\mathbf{R}}V_{ij}(\mathbf{r},\mathbf{R}), \tag{28}$$

where $c_{0i}(\mathbf{r},\mathbf{R})$ are elements of the vector $\mathbf{c}_0(\mathbf{r},\mathbf{R})$ given in equation (6) and $V_{ij}(\mathbf{r},\mathbf{R})$ are the EVB matrix elements. For fully variational multiconfigurational wavefunctions (i.e. when the wavefunction is optimized for each individual state), the Hellmann–Feynman forces are exact [105]. Note that the multiconfigurational wavefunctions obtained with the state-averaged FGH-MCSCF method described in [59] are not fully variational for each individual state. Thus, when using the FGH-MCSCF approach, a sufficient number of configurations must be included to ensure that the inaccuracies of the Hellmann–Feynman forces due to state averaging are negligible.

The quantum amplitudes $C_n(t)$ are obtained by integrating the time-dependent Schrödinger equation simultaneously with the classical equations of motion. Substitution of equation (25) into the time-dependent Schrödinger equation leads to

$$i\hbar\dot{C}_k(t) = \sum_{n=0}^{N_{\mathrm{ad}}-1} C_n(t)[\epsilon_k(\mathbf{R})\delta_{nk} - \mathrm{i}\hbar\dot{\mathbf{R}}\cdot\,\mathbf{d}_{kn}(\mathbf{R})], \tag{29}$$

where the non-adiabatic coupling vector $\mathbf{d}_{kn}$ is defined as

$$\mathbf{d}_{kn}(\mathbf{R}) \equiv \langle\Phi_k|\nabla_{\mathbf{R}}\Phi_n\rangle_{\mathbf{r}} = \frac{\langle\Phi_k|\nabla_{\mathbf{R}}V_{\mathrm{el0}}(\mathbf{r},\mathbf{R})|\Phi_n\rangle_{\mathbf{r}}}{\epsilon_n - \epsilon_k}. \tag{30}$$

At each time step, Tully's [60] 'fewest-switches' algorithm is invoked to determine whether a quantum transition to another adiabatic state should occur. This algorithm correctly apportions trajectories among the adiabatic states according to the quantum probabilities $|C_n(t)|^2$ with the minimum required number of quantum transitions (neglecting difficulties with classically forbidden transitions). According to this algorithm, the probability of switching from the current state k to another state n during the time interval between t and $t+\delta t$ is

$$g_{kn} = \max\left(0, \frac{-2\ \mathrm{Re}[C_k^*(t)C_n(t)\dot{\mathbf{R}}\cdot\mathbf{d}_{nk}]\delta t}{|C_k(t)|^2}\right). \tag{31}$$

A uniform random number is selected at each time step to determine if a switch to any state n will occur. If a switch to a different state n does occur, then the velocities must be adjusted to conserve energy. The velocities are adjusted as if they were subjected to a force in the direction of the non-adiabatic coupling vector. If there is not enough velocity in the direction of the non-adiabatic coupling vector to maintain energy conservation, the system remains in the initial quantum state. Various prescriptions for these so-called 'classically forbidden transitions' have been proposed. The options include the following: maintain the original velocities, reverse the velocities in the direction of the non-adiabatic coupling vector [50], or alter the integration of the time-dependent Schrödinger equation to eliminate completely these classically forbidden transitions [79,106]. For the application presented in [56], the optimal prescription was determined to be to maintain the original velocities.

2.3.3. *Combining the molecular dynamics with quantum transitions method with the reactive flux approach*

The use of the standard classical reactive flux approach in conjunction with MDQT is problematic since the probability of non-adiabatic transitions depends on the quantum amplitudes, which depend on the history of the trajectory. Thus, trajectories started at the dividing surface cannot be propagated backwards in time with the MDQT method. (Backward propagation requires knowledge of the quantum amplitudes at the dividing surface, which are unavailable.) In order to address this problem, Hammes-Schiffer and Tully [107] developed a non-adiabatic transition state theory that serves as the basis of a new method for simulating infrequent events in reactions that evolve on multiple potential energy surfaces. In this approach, trajectories are started at the dividing surface and propagated backwards in time with a 'fictitious' surface hopping algorithm that does not depend on the quantum amplitudes. The trajectory is then propagated forwards in time, retracing the exact same trajectory, integrating the quantum amplitudes and calculating the probabilities for non-adiabatic transitions for each time step using the true surface hopping algorithm. Each trajectory is assigned a weighting that ensures that the overall results are identical with those that would have been obtained with the true surface hopping algorithm.

In the implementation of this reactive flux method for MDQT within the framework of the methodology presented in this paper,

$$\kappa = \frac{\sum_{i=1}^{N_{\mathrm{traj}}}(\dot{\mathbf{R}}_i\cdot\hat{\mathbf{n}}_i)w_i^{\mathrm{can}}w_i^{\mathrm{sh}}\xi}{\sum_{i=1}^{N_{\mathrm{traj}}}(\dot{\mathbf{R}}_i\cdot\hat{\mathbf{n}}_i)w_i^{\mathrm{can}}w_i^{\mathrm{sh}}}. \tag{32}$$

Here N_{traj} is the number of trajectories required to represent an ensemble, $\dot{\mathbf{R}}_i$ is the initial velocity vector, $\hat{\mathbf{n}}_i$ is the normal to the dividing surface, w_i^{can} is the weighting to ensure a canonical distribution at the dividing surface and w_i^{sh} is the weighting to ensure the correct surface hopping probabilities for trajectory i. For the dividing surface defined as $\Lambda^{(\mathrm{q})}(\mathbf{R}) = 0$, the normal to the dividing surface is

$$\hat{\mathbf{n}}_i = \frac{\nabla_{\mathbf{R}}\Lambda^{(\mathrm{q})}(\mathbf{R}_i)}{|\nabla_{\mathbf{R}}\Lambda^{(\mathrm{q})}(\mathbf{R}_i)|}, \tag{33}$$

where

$$\nabla_{\mathbf{R}} A^{(q)}(\mathbf{R}) = \langle \Phi_0 | \nabla_{\mathbf{R}} [V_{22}(\mathbf{r},\mathbf{R}) - V_{11}(\mathbf{r},\mathbf{R})] | \Phi_0 \rangle_{\mathbf{r}} + 2 \sum_{n \neq 0}^{N_{ad}-1} \langle \Phi_0 | [V_{22}(\mathbf{r},\mathbf{R}) - V_{11}(\mathbf{r},\mathbf{R})] | \Phi_n \rangle_{\mathbf{r}} \mathbf{d}_{n0}. \quad (34)$$

For an ensemble of trajectories initiated at the dividing surface (i.e. configurations with $A^{(q)}(\mathbf{R}) = 0$ generated with the mapping potential $V_{map}(\mathbf{r},\mathbf{R};\lambda_m = 0.5)$),

$$w_i^{can} = \exp\{-\beta[\epsilon_k(\mathbf{R}_i) - V_{intmap}(\mathbf{R}_i;\lambda_m = 0.5)]\}, \quad (35)$$

where k is the vibrational adiabatic state occupied at the dividing surface. (Here we assume a Boltzmann distribution of the vibrational adiabatic states at the dividing surface.)

The weightings w_i^{sh} are obtained from the backward propagation with the fictitious surface hopping algorithm and the subsequent forward propagation over the exact same trajectory while integrating the quantum amplitudes and calculating the probabilities of non-adiabatic transitions for the true surface hopping algorithm. (Note that the quantum amplitudes for the forward propagation are initialized such that the quantum amplitude of the occupied state after the backward propagation is unity.) The weighting may be expressed as

$$w_i^{sh} = \prod_{\mu=1}^{\tau} \omega_\mu, \quad (36)$$

where $\prod_{\mu=1}^{\tau}$ is over all time steps during the backward propagation and

$$\omega_\mu = \frac{g_{kn}}{f_{kn}} \text{ if a transition from state } k \text{ to state } n \text{ was attempted}$$
$$= \left(1 - \sum_{n \neq k}^{N_{ad}-1} g_{kn}\right) \Bigg/ \left(1 - \sum_{n \neq k}^{N_{ad}-1} f_{kn}\right) \text{ if no transition was attempted.} \quad (37)$$

Here g_{kn} and f_{kn} are the probabilities of a non-adiabatic transition from k to j for the true and fictitious surface hopping algorithms respectively. One possible functional form for f_{kn} is

$$f_{kn} = \eta[1 - \exp(-|\dot{\mathbf{R}} \cdot \mathbf{d}_{kn}|\delta t)], \quad (38)$$

where η is a constant typically set to 0.5. The true surface hopping probability g_{kn} (given in equation (31)) for Tully's [60] fewest switches algorithm depends on the quantum amplitudes, while the fictitious probability f_{kn} does not. Note that this weighting procedure is based on the assumption that both the fictitious and the true MDQT surface hopping algorithms result in exact Boltzmann distributions among the vibrational states for long times (i.e. after equilibration of the reactant or product). This assumption is not rigorously valid, and the impact of this approximation is currently under investigation.

2.3.4. *Extensions of the dynamical formulation*

The basic principle of propagating trajectories backwards with a 'fictitious' algorithm and weighting the trajectories accordingly to obtain results identical with those that would have been obtained with a particular mixed quantum–classical

method is general. Thus, this basic approach may be extended for use with other mixed quantum–classical molecular dynamics methods. The combination of the adiabatic method with the reactive flux scheme is straightforward since the propagation of the quantum amplitudes is not required. The procedure would be identical with that described above except that the system would remain in a single vibrational adiabatic state and the weighting $w_i^{sh} = 1$. The combination of the mean field method with the reactive flux scheme is more challenging since the quantum amplitudes at the dividing surface are required for backward propagation of the trajectories. One possible prescription would be to initiate the trajectories in pure adiabatic states at the dividing surface and to propagate the amplitudes backward in time according to the time-dependent Schrödinger equation, allowing the classical subsystem to move according to an average path obtained from the mixture of adiabatic states. The weighting w_i^{sh} would then be determined according to the overlap of the resulting time-dependent wavefunction with a pure adiabatic state for the reactant. The combination of the reactive flux scheme with an approach that mixes surface hopping and mean field methods would require a more complicated prescription.

3. Applications

3.1. *Hydride transfer in enzymes*

The initial application of the approach described in this review centred on hydride transfer in the enzyme LADH. The mechanism of LADH involves both a hydride transfer between the alcohol substrate and the NAD^+ cofactor and a proton transfer from the substrate to the external solvent through a proton relay. Previous electronic structure and classical forcefield calculations [108] imply that the proton transfer occurs prior to the hydride transfer. Thus, the initial dynamical study [56] focused on only the hydride transfer reaction after the proton relay, that is hydride transfer from the alkoxide substrate to the NAD^+ cofactor. A portion of the active site of LADH for this hydride transfer reaction is depicted in figure 1.

In [56], the hydride transfer reaction in LADH was described in terms of a two-state EVB model. In the first VB state, the hydride is bonded to the substrate (i.e. the reacting complex is composed of benzyl alkoxide and NAD^+); in the second VB state, the hydride is bonded to the cofactor (i.e. the reacting complex is composed of benzaldehyde and NADH). The diagonal elements of the EVB Hamiltonian were described by a modified version of the GROMOS force field 43A1 [109]. The coupling and energy difference between the two VB states were assumed to be constant and were chosen to ensure that the quantum free energy profile for the reaction reproduced the experimental free energies of reaction and activation.

The free energy profiles and transmission coefficients calculated with the approach described above provide insight into the significance of nuclear quantum effects. An example of a hydrogen vibrational wavefunction for a transition state of the hydride transfer reaction in LADH is depicted in figure 2. The delocalization of the wavefunction between the donor and acceptor carbon atoms provides an indication that nuclear quantum effects are significant. Further evidence is given by the classical and quantum free energy profiles shown in figure 3. Since the free energy associated with the zero point motion is smaller for the transition state than for the reactant and product, the nuclear quantum effects substantially decrease the free energy barrier for this reaction. The calculated transmission coefficient κ

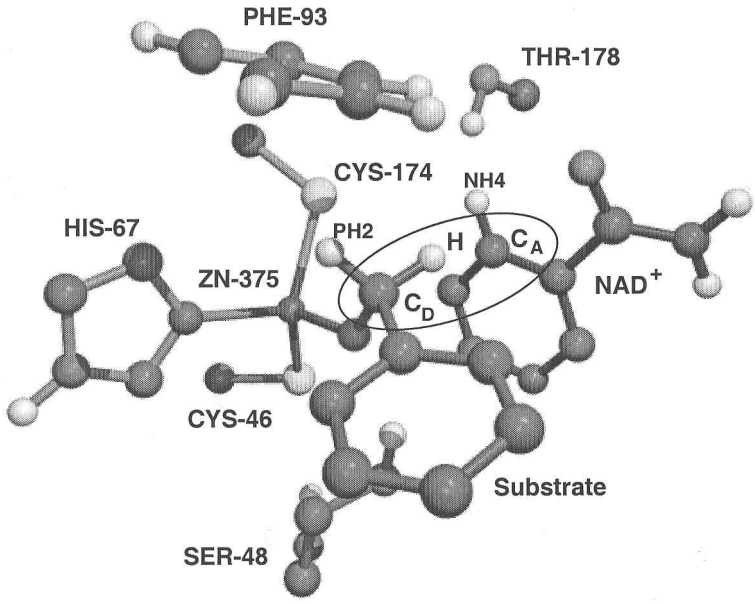

Figure 1. Portion of the active site of LADH, where C_D and C_A denote the donor and acceptor carbon atoms respectively.

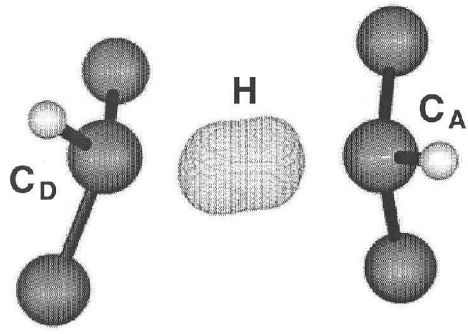

Figure 2. Depiction of a three-dimensional hydrogen vibrational wavefunction for a transition state of the hydride transfer reaction in LADH.

(including vibrationally non-adiabatic effects) is nearly unity, suggesting that dynamical effects are not significant for this reaction.

These simulations also provide insight into the physical basis for the observed kinetic isotope effects for LADH. The quantum free energy profiles for the transfer of hydrogen, deuterium and tritium are given in figure 4. As expected, the free energy barrier is lowest for hydrogen and highest for tritium. The kinetic isotope effects resulting from these different free energy barriers are in agreement with experimentally measured values. The calculated transmission coefficients κ for hydrogen and deuterium are similar, suggesting that the kinetic isotope effect for LADH arises mainly from differences in the free energy barrier rather than the dynamics.

This hybrid approach also allowed the analysis of individual real-time dynamical reactive trajectories and a statistical ensemble of such trajectories for LADH. Figure 5 depicts three representative trajectories for which the dividing surface is

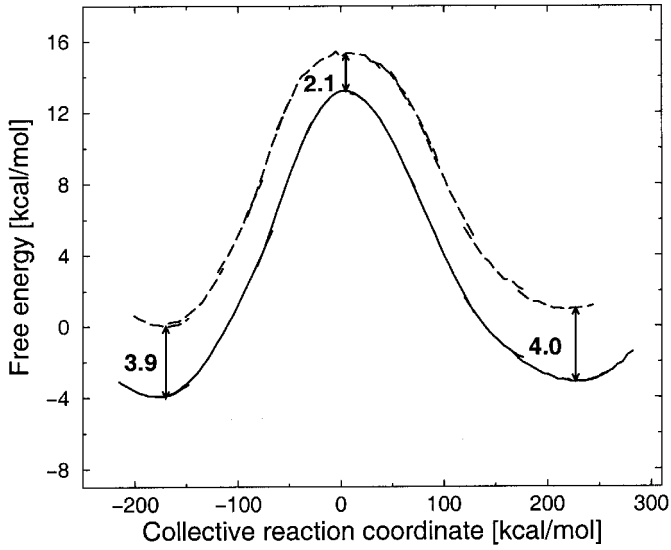

Figure 3. Classical (——) and quantum (- - - -) free energy profiles for hydride transfer in LADH.

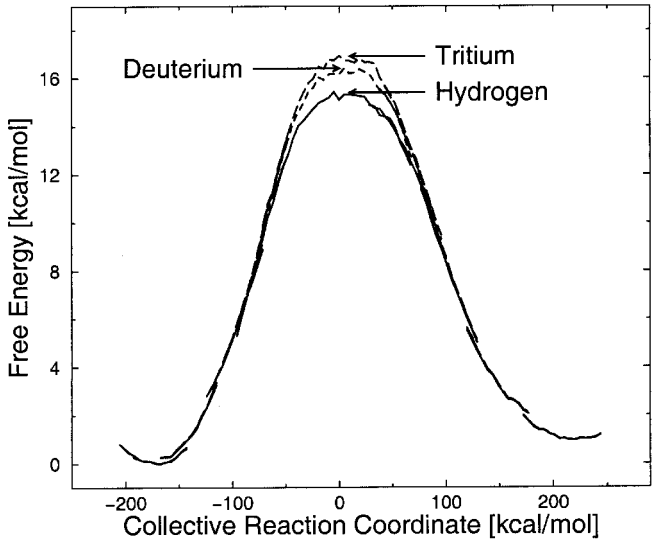

Figure 4. Quantum free energy profiles for the transfer of hydrogen (——), deuterium (- - - -), and tritium (– – –) in LADH.

chosen to be $\Lambda^{(q)} = 0$. Figure 5(*a*) illustrates a reactive trajectory that exhibits only a single crossing of the dividing surface, while figure 5(*b*) illustrates a non-reactive trajectory that crosses the dividing surface once in the forward direction and once in the backward direction. Figure 5(*c*) illustrates a reactive trajectory that crosses the dividing surface twice in the forward direction and once in the backward direction. Note that figures 5(*a*) and (*b*) do not exhibit any non-adiabatic transitions, while figure 5(*c*) exhibits a non-adiabatic transition near the dividing surface. In [110], a detailed analysis of both the equilibrium simulations and the real-time dynamical

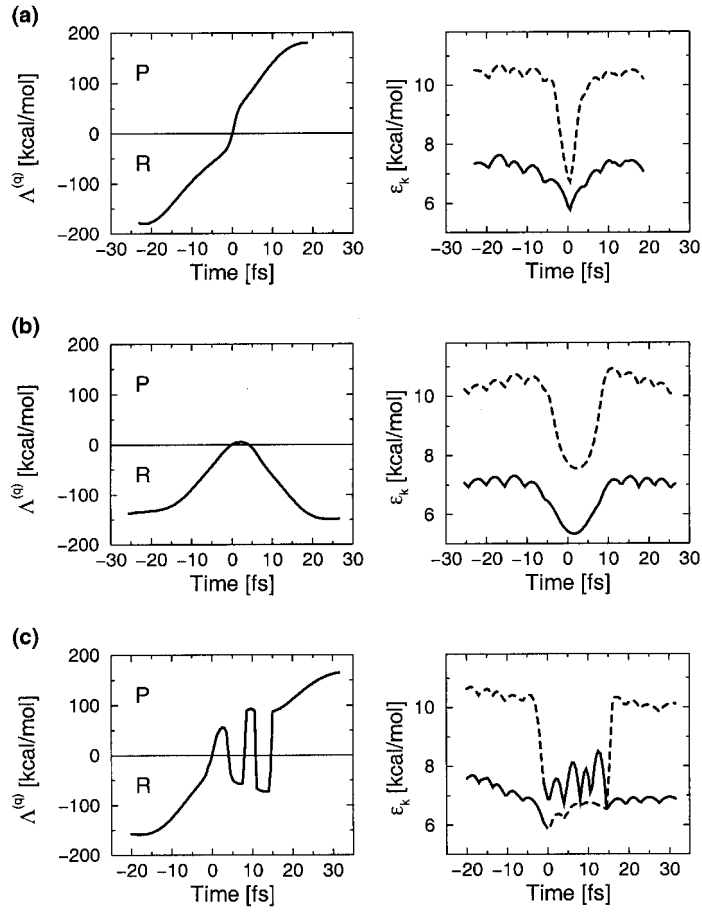

Figure 5. Three representative dynamical trajectories for hydride transfer in LADH: (*a*) reactive trajectory; (*b*) non-reactive trajectory; (*c*) reactive trajectory with a non-adiabatic transition and recrossings of the barrier. The time evolution of the quantum reaction coordinate is shown on the left, and the time evolution of the energies of the lowest two hydrogen vibrational states is shown on the right (where the occupied state is indicated by a solid line).

trajectories was performed to determine the relation between specific enzyme motions and enzyme activity. The analysis of the equilibrium simulations provided an indication of which geometrical properties impact the activation free energy barrier. The analysis of the real-time dynamical trajectories provided an indication of which geometrical properties impact the transmission coefficient (i.e., were correlated to the degree of dynamical recrossing of the barrier). The investigation of the impact of protein mutations will provide additional information about the relation between enzyme motion and function.

3.2. *Double proton and proton-coupled electron transfer*

Within the VB formulation [94], a process involving N charge transfer reactions may be described in terms of 2^N VB states and N linearly independent collective reaction coordinates. Thus, double proton transfer and PCET reactions may be described in terms of four VB states and two collective reaction coordinates.

3.2.1. *Double proton transfer*

Figure 6 depicts the four relevant VB states for double proton transfer in the formamidine-formic acid dimer. (Note that this VB model was introduced for a similar double proton transfer interface in [111].) If the reactant corresponds to the *aa* VB state, the physically meaningful collective reaction coordinates are

$$\begin{aligned} z_{\mathrm{p1}} &= \langle \Phi_0(\mathbf{r};\mathbf{R}) | V_{ba}(\mathbf{r},\mathbf{R}) - V_{aa}(\mathbf{r},\mathbf{R}) | \Phi_0(\mathbf{r};\mathbf{R}) \rangle_{\mathbf{r}} \\ z_{\mathrm{p2}} &= \langle \Phi_0(\mathbf{r};\mathbf{R}) | V_{ab}(\mathbf{r},\mathbf{R}) - V_{aa}(\mathbf{r},\mathbf{R}) | \Phi_0(\mathbf{r};\mathbf{R}) \rangle_{\mathbf{r}}, \\ z_{\mathrm{p3}} &= \langle \Phi_0(\mathbf{r};\mathbf{R}) | V_{bb}(\mathbf{r},\mathbf{R}) - V_{aa}(\mathbf{r},\mathbf{R}) | \Phi_0(\mathbf{r};\mathbf{R}) \rangle_{\mathbf{r}}. \end{aligned} \tag{39}$$

As shown in [94], within the VB formulation these three reaction coordinates are not linearly independent:

$$z_{\mathrm{p3}} = z_{\mathrm{p1}} + z_{\mathrm{p2}}. \tag{40}$$

Thus, the free energy profiles may be obtained as functions of only two of these three collective coordinates (i.e. z_{p1} and z_{p2}). For electronically adiabatic double proton transfer, the electronic ground state $V_{\mathrm{el0}}(\mathbf{r},\mathbf{R})$ is obtained by diagonalizing the 4×4 EVB Hamiltonian matrix. The mapping potential required to drive this reaction over the barrier could be defined as in equation (12) using the two VB states *aa* and *bb*. If adequate sampling requires a weighting of the intermediate VB states *ab* and *ba*, this expression for the mapping potential could be extended to include more mapping

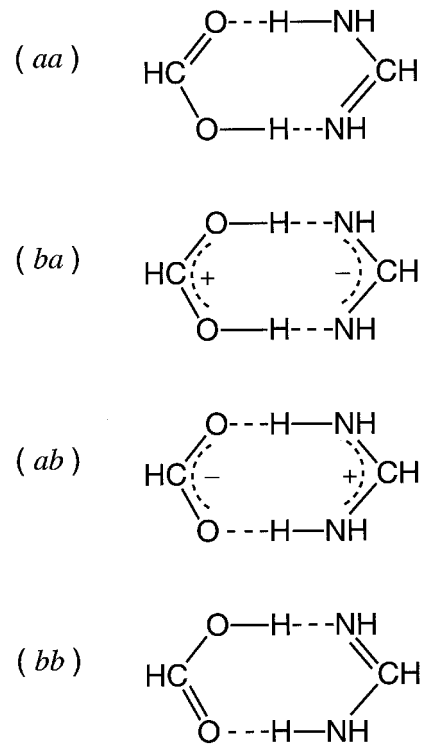

Figure 6. The four VB states for double proton transfer in the formamidine–formic acid dimer.

parameters and more VB states. Alternatively, a two-dimensional umbrella potential (analogous to equation (24)) could be introduced to sample the full range of relevant collective reaction coordinates z_{p1} and z_{p2}.

The procedure for calculating the free energy surfaces and transmission coefficients is analogous to that described above. For the calculation of the two-dimensional free energy surfaces, the function $\delta(\Lambda^{(q)} - \Lambda_n)$ is replaced by the product $\delta(z_{p1} - z_{p1}^{(m)})\delta(z_{p2} - z_{p2}^{(n)})$, and the quantities in angular brackets are calculated within two-dimensional bins. The transition state theory rate constant k_{TST} may be calculated using multidimensional transition state theory or Grote–Hynes [112] theory (see also [113, 114]). If there are multiple minima, the individual reactions may be treated independently and then combined according to an appropriate kinetic scheme. This approach allows the description of both sequential and concerted mechanisms. For the calculation of the transmission coefficient, the dividing surface must be chosen appropriately for each reaction in the two-dimensional space.

Figure 7 depicts double proton transfer along a water chain. In this case, a three-state VB model is adequate, where the extra proton resides on one of the three water molecules in each VB state. Multistate VB models for an extra proton in water have been developed by Vuilleumier and Borgis [115, 116] and by Schmitt and Voth [31, 117]. As for the formamidine–formic acid dimer, the free energy surfaces may be calculated as functions of two collective coordinates, and the transition state theory rate constant and transmission coefficient may be calculated in the same manner as described above. In related studies, the MDQT method has been applied to proton transfer along water chains using the Stillinger potential [57, 58]. In this case, the methods for infrequent events were not required since the reaction was driven by an electric field or by non-equilibrium initial conditions. These simulations indicate the significance of nuclear quantum effects and non-adiabatic transitions in water chains. The methodology presented in this review will allow further investigation of these types of multiple proton transfer reaction.

3.2.2. *Proton-coupled electron transfer*

Figure 8 depicts the four VB states for a PCET reaction between iron bi-imidazoline complexes [118]. In the notation for the VB states, 1 and 2 denote the electron transfer (ET) state, and *a* and *b* denote the proton transfer state. In this case, the physically meaningful collective coordinates are

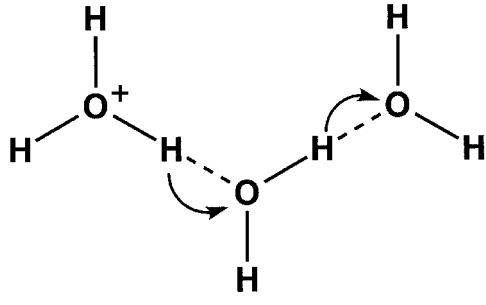

Figure 7. Protonated water trimer with arrows indicating the double proton transfer reaction.

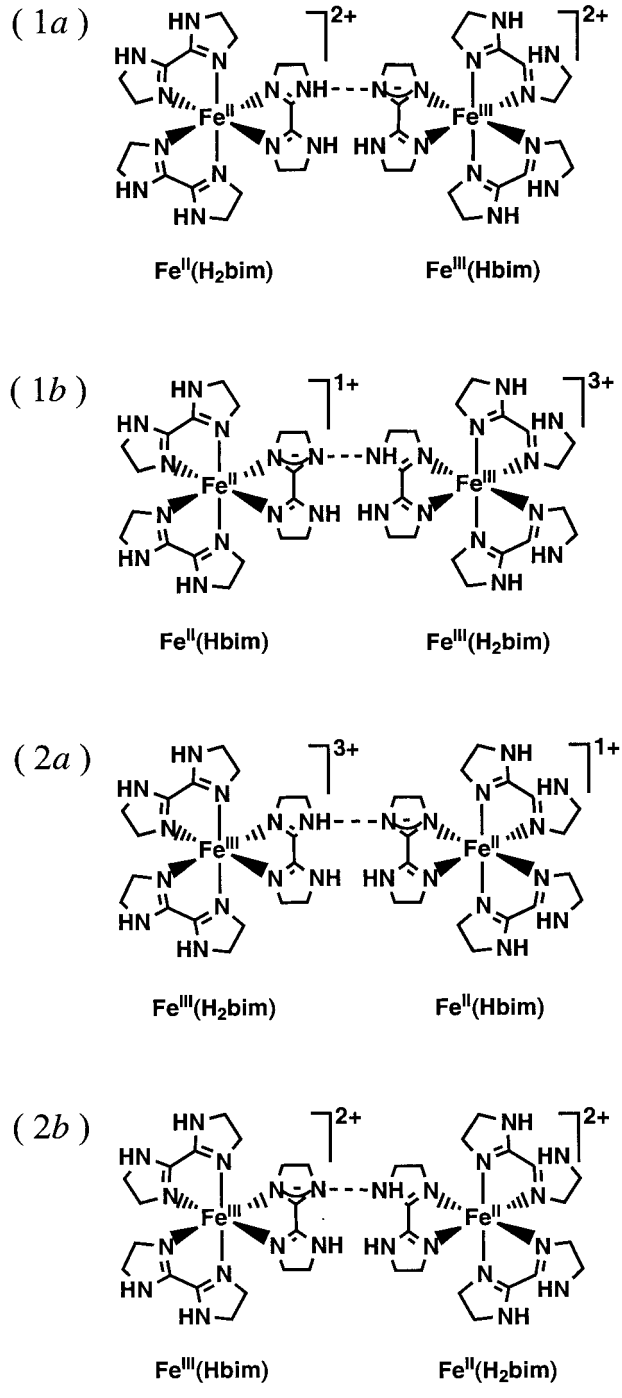

Figure 8. The four VB states for PCET between iron bi-imidazoline complexes.

$$z_{\mathrm{p}} = \langle \Phi_0(\mathbf{r};\mathbf{R}) | V_{1b}(\mathbf{r},\mathbf{R}) - V_{1a}(\mathbf{r},\mathbf{R}) | \Phi_0(\mathbf{r};\mathbf{R}) \rangle_{\mathbf{r}},$$
$$z_{\mathrm{e}} = \langle \Phi_0(\mathbf{r};\mathbf{R}) | V_{2a}(\mathbf{r},\mathbf{R}) - V_{1a}(\mathbf{r},\mathbf{R}) | \Phi_0(\mathbf{r};\mathbf{R}) \rangle_{\mathbf{r}}, \quad (41)$$
$$z_{\mathrm{ep}} = \langle \Phi_0(\mathbf{r};\mathbf{R}) | V_{2b}(\mathbf{r},\mathbf{R}) - V_{1a}(\mathbf{r},\mathbf{R}) | \Phi_0(\mathbf{r};\mathbf{R}) \rangle_{\mathbf{r}}.$$

Again, as shown in [94], within the VB formulation these three solvent coordinates are not linearly independent:

$$z_{\mathrm{ep}} = z_{\mathrm{p}} + z_{\mathrm{e}}. \quad (42)$$

Thus, the free energy surfaces should be obtained as functions of only two of these three collective coordinates (i.e. z_{p} and z_{e}).

For PCET reactions such as that shown in figure 8, typically the electron transfer reaction is electronically non-adiabatic, while the proton transfer reaction is electronically adiabatic. Thus, the relevant free energy surfaces are the two sets of ET diabatic surfaces corresponding to the two ET VB states 1 and 2. These surfaces are obtained by diagonalizing two separate 2×2 EVB Hamiltonian matrices (corresponding to $1a$-$1b$ and $2a$-$2b$, respectively). ET diabatic free energy surfaces depending on z_{p} and z_{e} have been obtained for PCET reactions using a multistate continuum theory, in which the solvent is represented as a dielectric continuum [118–120]. Furthermore, recently these two-dimensional free energy surfaces have been obtained for a model PCET reaction in solution using molecular dynamics methods with explicit solvent molecules [121]. The rates for PCET reactions have been calculated by the application of the golden rule to the two sets of ET diabatic free energy surfaces [120, 122].

The two-dimensional ET diabatic free energy surfaces and the dynamical transmission coefficient may be calculated with the formulation presented in this review. As for double proton transfer, a two-dimensional umbrella potential may be introduced to sample the full range of relevant collective solvent coordinates z_{p} and z_{e}. Alternatively, the mapping potential could be used to sample the full range of z_{p} for each ET state, and an umbrella potential could be introduced to sample the full range of z_{e}. Analogous to the extension for double proton transfer, $\delta(\Lambda^{(\mathrm{q})} - \Lambda_n)$ is replaced by the product $\delta(z_{\mathrm{p}} - z_{\mathrm{p}}^{(m)})\delta(z_{\mathrm{e}} - z_{\mathrm{e}}^{(n)})$, and the quantities in angular brackets are calculated within two-dimensional bins. This approach allows the investigation of the free energy surfaces for PCET in proteins as well as solution. (Note that, under a set of well-defined and physically reasonable conditions, this approach is equivalent to that used in [121] to obtain two-dimensional ET diabatic free energy surfaces.) Dynamical effects may be included by initiating trajectories near the non-adiabatic crossings of the two sets of ET diabatic free energy surfaces. This is a direction for future research.

4. Conclusions

This review summarizes a hybrid approach for the real-time dynamical simulation of proton and hydride transfer reactions in solution and proteins. The electronic quantum effects are incorporated with an EVB potential that allows the relevant bonds to break and form. The nuclear quantum effects of the transferring hydrogen are included with a mixed quantum–classical approach that represents the transferring hydrogen nucleus by a three-dimensional wavefunction. The free energy profiles are obtained as functions of a collective reaction coordinate using a mapping or

umbrella potential to drive the reaction over the barrier. The vibrationally adiabatic nuclear quantum effects are incorporated into these free energy profiles. The dynamical effects are described with the MDQT surface hopping method, which incorporates non-adiabatic transitions among the adiabatic hydrogen vibrational states. The MDQT method is combined with a reactive flux method to allow the calculation of the dynamical transmission coefficient and the investigation of the real-time dynamics of reactive trajectories.

This hybrid approach is very powerful for a number of reasons. Nuclear quantum effects such as zero point energy, hydrogen tunnelling, and non-adiabatic transitions among vibrational states are incorporated in a computationally practical manner. These nuclear quantum effects are included during the generation of the free energy profiles and dynamical trajectories rather than added as corrections to classical simulations. The dynamical motion of the complete environment (i.e. solvent and/or protein) is included in these calculations. The resulting real-time dynamical reactive trajectories provide detailed mechanistic information at the molecular level. An analysis of geometrical properties during the equilibrium and dynamical simulations provides insight into the relation between specific enzyme motions and enzyme activity. Furthermore, this approach allows the calculation of rates and kinetic isotope effects for comparison with experiment and for predictive purposes.

The computational feasibility of this approach has been illustrated through the application to hydride transfer in the enzyme LADH. In this application, the transferring hydride is treated as a three-dimensional vibrational wavefunction, and the classical subsystem includes more than 75 000 atoms. The calculated kinetic isotope effects agree with experimental data. The dynamical transmission coefficients were found to be nearly unity, indicating only a small contribution from dynamical recrossings of the barrier. Individual reactive trajectories were analysed to provide insight into the detailed mechanism. In addition, a statistical ensemble of trajectories was analysed to determine correlations between geometrical properties of the system and the degree of dynamical recrossing of the barrier. These correlations provide insight into the relation between enzyme dynamics and function. The investigation of the impact of protein mutations on these correlations, as well as on the free energy barrier and transmission coefficient, will provide further insight into this relation.

This hybrid approach may be extended in a variety of directions. For example, the EVB potential could be replaced by a QM–MM potential based on semiempirical or *ab initio* electronic structure methods. In this case, an umbrella potential may be used to drive the reaction over the barrier. A multistate EVB potential has been implemented for multiple charge transfer reactions such as double proton transfer and proton-coupled ET. Within the VB description, the free energy profiles for a process involving N charge transfer reactions depends on N linearly independent collective reaction coordinates. This formulation provides information about the detailed mechanism, such as whether the charge transfer reactions are concerted or sequential. Grid methods have been developed for the efficient calculation of the multidimensional vibrational wavefunctions required for the QM treatment of multiple hydrogen nuclei. These grid methods may also be used to treat additional modes, such as the proton donor–acceptor vibration, quantum mechanically at the same level as the transferring hydrogen nucleus. Another possible extension is to replace the MDQT surface hopping method with an alternative non-adiabatic molecular dynamics method. The specific procedure for propagating trajectories

backward from the transition state without *a priori* knowledge of the quantum amplitudes must be modified for different non-adiabatic molecular dynamics methods.

As a result of the flexibility and computational efficiency of this hybrid approach, it is applicable to a wide range of proton and hydride transfer reactions. These types of simulation will enhance our understanding of the fundamental chemical and physical principles of charge transfer reactions. In addition, these simulations will elucidate the detailed mechanisms of biologically and chemically important processes.

Acknowledgements

We are grateful for financial support from National Institutes of Health grant GM56207 and National Science Foundation grant CHE-0096357. S.H.S. is the recipient of an Alfred P. Sloan Foundation Research Fellowship and a Camille Dreyfus Teacher–Scholar Award.

References

[1] Bahnson, B. J., and Klinman, J. P., 1995, *Meth. Enzymology*, **249**, 374.
[2] Kohen, A., and Klinman, J. P., 1998, *Accts. Chem. Res.*, **31**, 397.
[3] Kohen, A., Jonsson, T., and Klinman, J. P., 1997, *Biochemistry*, **36**, 2603.
[4] Kohen, A., Cannio, R., Bartolucci, S., and Klinman, J. P., 1999, *Nature*, **399**, 496.
[5] Miller, G. P., and Benkovic, S. J., 1998, *Chem. Biol.*, **5**, R105–R113.
[6] Olson, L. P., Luo, J., Almarsson, O., and Bruice, T. C., 1996, *Biochemistry*, **35**, 9782.
[7] Torres, R. A., Schiott, B., and Bruice, T. C., 1999, *J. Am. chem. Soc.*, **121**, 8164.
[8] Warshel, A., and Levitt, M., 1976, *J. molec. Biol.*, **103**, 227.
[9] Singh, U., and Kollman, P., 1986, *J. comput. Chem.*, **7**, 718.
[10] Field, M. J., Bash, P. A., and Karplus, M., 1990, *J. comput. Chem.*, **11**, 700.
[11] Aqvist, J., and Warshel, A., 1993, *Chem. Rev.*, **93**, 2523.
[12] Gao, J., 1996, *Accts. Chem. Res.*, **29**, 298.
[13] Warshel, A., 1991, *Computer Modeling of Chemical Reactions in Enzymes and Solutions*, (New York: Wiley).
[14] Warshel, A., 1982, *J. phys. Chem.*, **86**, 2218.
[15] Warshel, A., 1984, *Proc. natn. Acad. Sci. USA*, **81**, 444.
[16] Cunningham, M. A., Ho, L. L., Nguyen, D. T., Gillilan, R. E., and Bash, P. A., 1997, *Biochemistry*, **36**, 4800.
[17] Mo, Y. R., and Gao, J. L., 2000, *J. phys. Chem.* A, **104**, 3012.
[18] Warshel, A., and Chu, Z. T., 1990, *J. chem. Phys.*, **93**, 4003.
[19] Yadav, A., Jackson, R. M., Holbrook, J. J., and Warshel, A., 1991, *J. Am. chem. Soc.*, **113**, 4800.
[20] Hwang, J.-K., Chu, Z. T., Yadav, A., and Warshel, A., 1991, *J. phys. Chem.*, **95**, 8445.
[21] Hwang, J.-K., and Warshel, A., 1996, *J. Am. chem. Soc.*, **118**, 11 745.
[22] Li, D., and Voth, G. A., 1991, *J. phys. Chem.*, **95**, 10 425.
[23] Azzouz, H., and Borgis, D., 1993, *J. chem. Phys.*, **98**, 7361.
[24] Pomès, R., and Roux, B., 1995, *Chem. Phys. Lett.*, **234**, 416.
[25] Tuckerman, M., Laasonen, K., Sprik, M., and Parrinello, M., 1995, *J. chem. Phys.*, **103**, 150.
[26] Tuckerman, M. E., Marx, D., Klein, M. L., and Parrinello, M., 1997, *Science*, **275**, 817.
[27] Cao, J., and Voth, G. A., 1994, *J. chem. Phys.*, **100**, 5093.
[28] Cao, J., and Voth, G. A., 1994, *J. chem. Phys.*, **100**, 5106.
[29] Cao, J., and Voth, G. A., 1994, *J. chem. Phys.*, **101**, 6157.
[30] Cao, J., and Voth, G. A., 1994, *J. chem. Phys.*, **101**, 6168.

[31] SCHMITT, U., and VOTH, G. A., 1999, *J. chem. Phys.*, **111**, 9361.
[32] BEN-NUN, M., and MARTINEZ, T. J., 1999, *J. phys. Chem.* A, **103**, 6055.
[33] GUALLAR, V., BATISTA, V. S., and MILLER, W. H., 2000, *J. chem. Phys.*, **113**, 9510.
[34] TOPALER, M., and MAKRI, N., 1994, *J. chem. Phys.*, **101**, 7500.
[35] MAKRI, N., 1999, *A. Rev. phys. Chem.*, **50**, 167.
[36] MORILLO, M., and CUKIER, R. I., 1990, *J. chem. Phys.*, **92**, 4833.
[37] SUÁREZ, A., and SILBEY, R., 1991, *J. chem. Phys.*, **94**, 4809.
[38] TRUHLAR, D. G., LIU, Y.-P., SCHENTER, G. K., and GARRETT, B. C., 1994, *J. Phys. Chem.*, **98**, 8396.
[39] BORGIS, D., TARJUS, G., and AZZOUZ, H., 1992, *J. phys. Chem.*, **96**, 3188.
[40] BORGIS, D., TARJUS, G., and AZZOUZ, H., 1992, *J. chem. Phys.*, **97**, 1390.
[41] LARIA, D., CICCOTTI, G., FERRARIO, M., and KAPRAL, R., 1992, *J. chem. Phys.*, **97**, 378.
[42] STAIB, A., BORGIS, D., and HYNES, J. T., 1995, *J. chem. Phys.*, **102**, 2487.
[43] BORGIS, D., and HYNES, J. T., 1993, *Chem. Phys.*, **170**, 315.
[44] ANDO, K., and HYNES, J. T., 1995, *J. molec. Liquids*, **64**, 25.
[45] MAVRI, J., BERENDSEN, H. J. C., and VAN GUNSTEREN, W. F., 1993, *J. phys. Chem.*, **97**, 13 469.
[46] MAVRI, J., and BERENDSEN, H. J. C., 1995, *J. phys. Chem.*, **99**, 12 711.
[47] BALA, P., LESYNG, B., and MCCAMMON, J. A., 1994, *Chem. Phys.*, **180**, 271.
[48] BALA, P., GROCHOWSKI, P., LESYNG, B., and MCCAMMON, J. A., 1996, *J. phys. Chem.*, **100**, 2535.
[49] BALA, P., GROCHOWSKI, P., NOWINSKI, K., LESYNG, B., and MCCAMMON, J. A., 2000, *Biophys. J.*, **79**, 1253.
[50] HAMMES-SCHIFFER, S., and TULLY, J. C., 1994, *J. chem. Phys.*, **101**, 4657.
[51] HAMMES-SCHIFFER, S., and TULLY, J. C., 1995, *J. phys. Chem.*, **99**, 5793.
[52] HAMMES-SCHIFFER, S., 1998, *J. phys. Chem. A*, **102**, 10 443.
[53] LOBAUGH, J., and VOTH, G. A., 1992, *Chem. Phys. Lett.*, 198, 311.
[54] LOBAUGH, J., and VOTH, G. A., 1994, *J. chem. Phys.*, **100**, 3039.
[55] BILLETER, S. R., and VAN GUNSTEREN, W. F., 1997, *Comput. Phys. Commun.*, **107**, 61.
[56] BILLETER, S. R., WEBB, S. P., IORDANOV, T., AGARWAL, P. K., and HAMMES-SCHIFFER, S., 2001, *J. chem. Phys.*, **114**, 6925.
[57] DRUKKER, K., DE LEEUW, S., and HAMMES-SCHIFFER, S., 1998, *J. chem. Phys.*, **108**, 6799.
[58] DECORNEZ, H., DRUKKER, K., and HAMMES-SCHIFFER, S., 1999, *J. phys. Chem.* A, **103**, 2891.
[59] WEBB, S. P., and HAMMES-SCHIFFER, S., 2000, *J. chem. Phys.*, **113**, 5214.
[60] TULLY, J. C., 1990, *J. chem. Phys.*, **93**, 1061.
[61] TULLY, J. C., and PRESTON, R. K., 1971, *J. chem. Phys.*, **55**, 562.
[62] MILLER, W. H., and GEORGE, T. F., 1972, *J. chem. Phys.*, **56**, 5637.
[63] STINE, J. R., and MUCKERMAN, J. T., 1976, *J. chem. Phys.*, **65**, 3975.
[64] BLAIS, N. C., and TRUHLAR, D. G., 1983, *J. chem. Phys.*, **79**, 1334.
[65] DUNNE, L. J., MURRELL, J. N., and STAMPER, J. G., 1984, *Chem. Phys. Lett.*, **112**, 497.
[66] PARLANT, G., and GISLASON, E. A., 1989, *J. chem. Phys.*, **91**, 4416.
[67] PARLANT, G., and ALEXANDER, M. H., 1990, *J. chem. Phys.*, **92**, 2287.
[68] KUNTZ, P. J., 1991, *J. chem. Phys.*, **95**, 141.
[69] HERMAN, M. F., 1984, *J. chem. Phys.*, **81**, 754.
[70] ARCE, J. C., and HERMAN, M. F., 1994, *J. chem. Phys.*, **101**, 7520.
[71] WEBSTER, F., ROSSKY, P. J., and FRIESNER, R. A., 1991, *Comput. Phys. Commun.*, **63**, 494.
[72] COKER, D. F., and XIAO, L., 1995, *J. chem. Phys.*, **102**, 496.
[73] COKER, D. F., 1993, *Computer Simulation in Chemical Physics*, (Dordrecht: Kluwer).
[74] SCHWARTZ, B. J., BITTNER, E. R., PREZHDO, O. V., and ROSSKY, P. J., 1996, *J. chem. Phys.*, **104**, 5942.
[75] SHOLL, D. S., and TULLY, J. C., 1998, *J. chem. Phys.*, **109**, 7702.
[76] TOPALER, M. S., ALLISON, T. C., SCHWENKE, D. W., and TRUHLAR, D. G., 1998, *J. phys. Chem.* A, **102**, 1666.
[77] NIELSEN, S., KAPRAL, R., and CICCOTTI, G., 2000, *J. chem. Phys.*, **112**, 6543.
[78] WAN, C. C., and SCHOFIELD, J., 2000, *J. chem. Phys.*, **112**, 4447.

[79] FANG, J.-Y., and HAMMES-SCHIFFER, S., 1999, *J. chem. Phys.*, **110**, 11166.
[80] PREZHDO, O. V., and ROSSKY, P. J., 1997, *J. chem. Phys.*, **107**, 825.
[81] WONG, K. F., and ROSSKY, P. J., 2001, *J. phys. Chem.* A, **105**, 2546.
[82] ALHAMBRA, C., GAO, J. L., CORCHADO, J. C., VILLA, J., and TRUHLAR, D. G., 1999, *J. Am. chem. Soc.*, **121**, 2253.
[83] ALHAMBRA, C., CORCHADO, J. C., SANCHEZ, M. L., GAO, J., and TRUHLAR, D. G., 2000, *J. Am. chem. Soc.*, **122**, 8197.
[84] MARCUS, R. A., 1964, *A. Rev. phys. Chem.*, **15**, 155.
[85] ZUSMAN, L. D., 1980, *Chem. Phys.*, **49**, 295.
[86] KING, G., and WARSHEL, A., 1990, *J. chem. Phys.*, **93**, 8682.
[87] WIGNER, E., 1932, *Phys. Rev.*, **40**, 749.
[88] BENNETT, C. H., 1997, *Algorithms for Chemical Computation*, (Washington, D.C.: American Chemical Society).
[89] KECK, J. C., 1960, *J. chem. Phys.*, **32**, 1035.
[90] ANDERSON, J. B., 1973, *J. chem. Phys.*, **58**, 4684.
[91] EUKLUND, H., PLAPP, B. V., SAMAMA, J.-P., and BRANDEN, C., 1982, *J. biol. Chem.*, **257**, 14 359.
[92] RAMASWAMY, S., EKLUND, H., and PLAPP, B. V., 1994, *Biochemistry*, **33**, 5230.
[93] BAHNSON, B. J., PARK, D.-H., KIM, K., PLAPP, B. V., and KLINMAN, J. P., 1993, *Biochemistry*, **32**, 5503.
[94] SOUDACKOV, A. V., and HAMMES-SCHIFFER, S., 1999, *J. chem. Phys.*, **111**, 4672.
[95] LANCZOS, C., 1950, *J. Res. natu. Bur. Stand.*, **45**, 255.
[96] DAVIDSON, E. R., 1975, *J. comput. Phys.*, **17**, 87.
[97] LIGHT, J. C., HAMILTON, I. P., and LILL, J. V., 1984, *J. chem. Phys.*, **82**, 1400.
[98] MARSTON, C. C., and BALINT-KURTI, G. G., 1989, *J. chem. Phys.*, **91**, 3571.
[99] BACIC, Z., and LIGHT, J. C., 1989, *A. Rev. phys. Chem.*, **40**, 469.
[100] BRAMLEY, M. J., and CARRINGTON, T., 1993, *J. chem. Phys.*, **99**, 8519.
[101] YIN, J., and GREEN, M. E., 1998, *J. phys. Chem.* A, **102**, 7181.
[102] CARTER, S., BOWMAN, J., and HANDY, N. C., 1998, *Theor. Chem. Accts.*, **100**, 191.
[103] IORDANOV, T., BILLETER, S. R., WEBB, S. P., and HAMMES-SCHIFFER, S., 2001, *Chem. Phys. Lett.*, **338**, 389.
[104] ZWANZIG, R., 1954, *J. chem. Phys.*, **22**, 1420.
[105] DRUKKER, K., and HAMMES-SCHIFFER, S., 1997, *J. chem. Phys.*, **107**, 363.
[106] FANG, J.-Y., and HAMMES-SCHIFFER, S., 1999, *J. phys. Chem.* A, **103**, 9399.
[107] HAMMES-SCHIFFER, S., and TULLY, J. C., 1995, *J. chem. Phys.*, **103**, 8528.
[108] AGARWAL, P. K., WEBB, S. P., and HAMMES-SCHIFFER, S., 2000, *J. Am. chem. Soc.*, **122**, 4803.
[109] VAN GUNSTEREN, W. F., BILLETER, S. R., EISING, A. A., HÜNENBERGER, P. H., KRÜGER, P., MARK, A. E., SCOTT, W. R. P., and TIRONI, I. G., 1996, *Biomolecular Simulation: The GROMOS96 Manual and User Guide*, (Zürich: Biomos b.v., Zürich and Groningen, VdF Hochschulverlag, Eidgenössiche Technische Hochscule Zürich).
[110] BILLETER, S. R., WEBB, S. P., AGARWAL, P. K., IORDANOV, T., and HAMMES-SCHIFFER, S., 2001 (submitted).
[111] ROSTOV, I., and HAMMES-SCHIFFER, S., 2001, *J. chem. Phys.*, **115**, 285.
[112] GROTE, R. F., and HYNES, J. T., 1980, *J. chem. Phys.*, **73**, 2715.
[113] WEIDENMÜLLER, H. A., and JING-SHANG, Z., 1984, *J. statist. Phys.*, **34**, 191.
[114] HANGGI, P., TALKNER, P., and BORKOVEC, M., 1990, *Rev. mod. Phys.*, **62**, 251.
[115] VUILLEUMIER, R., and BORGIS, D., 1998, *Chem. Phys. Lett.*, **284**, 71.
[116] VUILLEUMIER, R., and BORGIS, D., 1998, *J. phys. Chem.* B, **102**, 4261.
[117] SCHMITT, U., and VOTH, G. A., 1998, *J. phys. Chem.* B, **102**, 5547.
[118] IORDANOVA, N., DECORNEZ, H., and HAMMES-SCHIFFER, S., 2001, *J. Am. chem. Soc.*, **123**, 3723.
[119] SOUDACKOV, A. V., and HAMMES-SCHIFFER, S., 1999, *J. Am. chem. Soc.*, **121**, 10 598.
[120] DECORNEZ, H., and HAMMES-SCHIFFER, S., 2000, *J. phys. Chem.* A, **104**, 9370.
[121] KOBRAK, M., and HAMMES-SCHIFFER, S., 2001, *J. phys. Chem.* B (to be published).
[122] SOUDACKOV, A. V., and HAMMES-SCHIFFER, S., 2000, *J. chem. Phys.*, **113**, 2385.